



Northeastern University

College of Science

Principles of Experimental Physics (PHYS5318)

Major Experiment Lab Report

Title: Synthesis and characterization of MnAl thin film

Anand Hari Natarajan and Harikumar Muthu

Professor: Dr. Don Heiman

Abstract

A MnAl ferromagnetic thin film sample was grown on a silicon substrate using DC magnetron sputtering and the effect of annealing on its magnetic properties was investigated using SQUID magnetometry. Additionally, SEM was used to examine the concentration of Mn and Al in the sample. Furthermore, a sample of Mn-MnAl thin film heterostructure was also grown on a silicon substrate to study magnetic anisotropy.

I. Introduction

Ferromagnetism is the physical phenomenon by which magnetic materials exhibit permanent magnetization and are strongly attracted to external magnetic fields. Ferromagnetism is the strongest kind of magnetism exhibited in magnetic materials; the others— paramagnetism, diamagnetism, and antiferromagnetism respond very weakly to external magnetic fields when compared with ferromagnetism.

Ferromagnetic materials show the property of **magnetic hysteresis** where if the material is placed in an external magnetic, its magnetic dipoles align with it. Even when the external field is removed, the alignment of the dipoles remains and the material becomes magnetic. The amount of magnetization retained in the material is called ‘remanence’. To demagnetize the material, an external magnetic field in the opposite direction must be applied to the material. The amount of external field required to demagnetize the material is called ‘coercivity’. The hysteresis loop for a given material is also called its ‘B-H curve’. Based on the hysteresis loop, a ferromagnetic material can be classified into ‘hard magnets’ and ‘soft magnets’. Hard magnets are those with high coercivity and therefore, a wide hysteresis loop. Soft magnets are those with low coercivity and thin hysteresis loop.

Ferromagnetism has a large number of applications in science and technology. The most widely used application is the element of **magnetic memory** in a magnetic hard disk drives, magnetic tapes, and credit cards. For these applications, hard magnets like iron are used. Other applications include transformer cores, electromagnets, motors, and generators. For these applications, soft magnets like soft iron, silicon-iron alloys, or mu-metals are used to boost the response of the coil.

Ferromagnetism in MnAl was first pointed out by Hindricks in 1908, and the **phase diagram** of the binary system was first analyzed by Hiroshi Kono in 1958 [1]. The MnAl system is found to be ferromagnetic when the percentage of Mn is about 50% to 60%. This phase is known as the **τ phase** and occurs in bulk materials at temperatures of about 500 °C to 800 °C. For MnAl thin films, the tau phase is usually produced by annealing the material to temperatures in the range of 400 °C to 450 °C [2].

Ferromagnetic materials can also be used to create devices that show interesting properties such as **exchange anisotropy**. Also called exchange bias, it is a kind of magnetic anisotropy, a property that measures how a material’s magnetic properties differ in various directions. This phenomenon occurs when an antiferromagnetic (AFM) material and ferromagnetic (FM) material are in contact and the system is cooled from high temperature through the Néel temperature of the AFM in an external magnetic field [3]. This effect is used in magnetic recording, where the readheads consist of a magnetic spin-valve: a device with two FM layers separated by a non-magnetic conductor.

II. Materials and Methods

A. Materials

The various processes used in this experiment to grow the thin-films and analyze their magnetic properties are DC Magnetron Sputtering, Annealing, SQUID magnetometry, and Scanning Electron Microscopy (SEM). Each process has its own experimental setup as discussed below.

A. I. Physical Vapor Deposition (DC magnetron sputtering)

Sputtering is the process by which atoms of selected materials are ejected off their surface by bombarding them with energized **plasma**. This process is used to grow thin films on substrates for a variety of applications. Here, DC magnetron sputtering was used to grow thin films of MnAl and Mn-MnAl on a silicon substrate. Usually for this process to work, the chamber is first evacuated to high vacuum and the sputtering gas is let into the chamber at a controlled rate. To start the plasma generation, a high voltage is applied between the cathode (located directly behind the target) and the anode (usually connected to the chamber as an electrical ground) [4]. In magnetron sputtering, a permanent magnet structure is located behind the deposition source material, called the ‘target’ (Figure 1) [5]. The generated plasma is confined and localized to the space containing the target due to the permanent magnet structure. The resulting magnetic field causes electrons ejected from the target to take a cycloidal trajectory, trapping them and greatly increasing the probability of **ionization** of the sputtering gas. The electrons following the cycloidal path collide with more sputtering gas atoms thereby causing secondary electrons to get ejected from the gas atoms. The positively charged gas atoms now get accelerated to the negatively charged cathode which is behind the target. Thus, the gas atoms collide with the surface of the target, which causes target atoms to get ejected and migrate to the substrate.

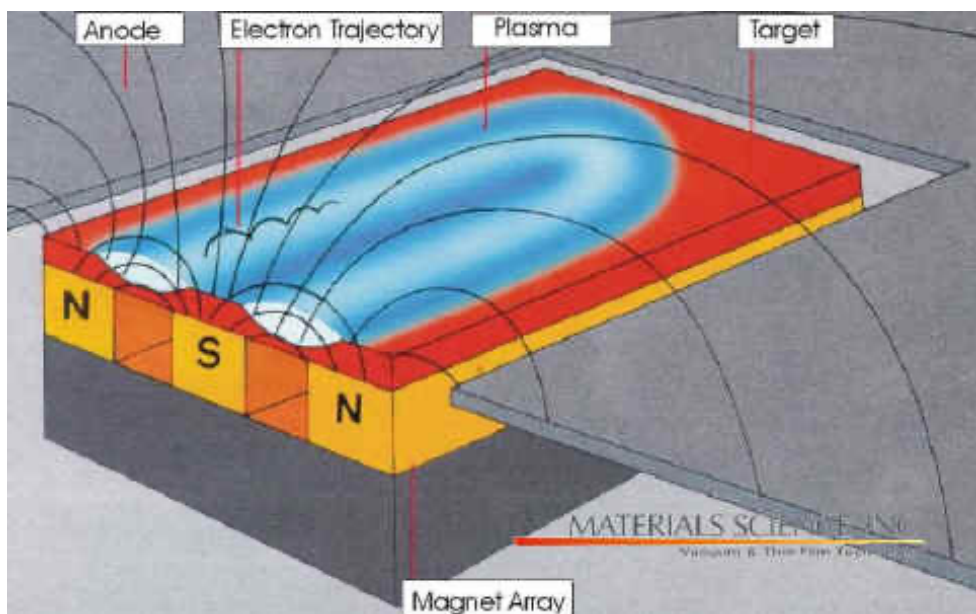


Figure 1: Mechanism of Magnetic Sputtering [5]

A. I. a. Experimental setup

A schematic diagram of the experimental setup for the sputtering process is shown in Figure 2. Pictures of the instruments are available in the Appendix.

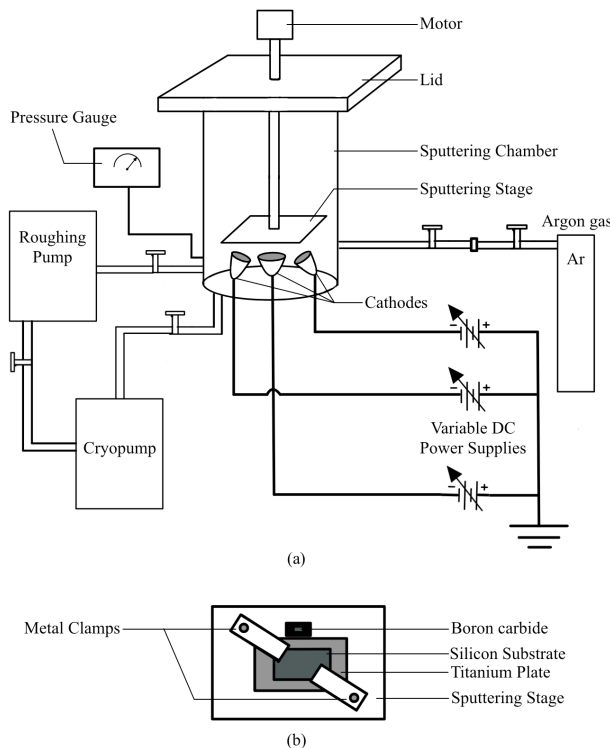


Figure 2: Schematic Diagram of the experimental setup for the Sputtering Process

The **sputtering chamber** is a large hollow glass cylinder with a metal wire mesh surface. It is used to house the substrate and cathodes used for the process. The chamber has a square shaped metal lid with a long metal rod through a hole in its centre. The rod is connected on one end to the sputtering stage via a screw and on the other end to a 10 rpm, 12 V DC motor, which is used to rotate the rod and stage. The sputtering stage also has metal clamps for fastening the sample as it will be held upside down for the duration of the deposition process.

The **roughing pump** is used to ‘rough out’ the vacuum chamber or remove unwanted residue from the chamber and is used as a first stage towards producing ultra high vacuum. For this purpose, the Leybold Trivac D25B 60 Hz vacuum pump is used. It is a durable dual stage rotary vane mechanical vacuum pump that provides a pressure of 1×10^{-4} torr. The unwanted residue can range from magnetic particles to hydroxide ions from moisture that is stuck to the walls of the chamber.

The **cryopump** is used to provide the vacuum inside the vacuum chamber. It works by cooling down gases and vapors to the point that the molecules condense on the chamber walls and get trapped. The cryopump used here is the CTI-Cryogenics Cryo-Torr 100. Fast and clean pumping of all gases are provided by this cryopump in the 10^{-3} to 10^{-9} torr range.

To monitor the pressure inside the vacuum chamber, two **pressure gauges** are used. The first one is a MKS 270A Signal Conditioner Vacuum Gauge with sensor range varying from 1 to 10K and resolution varying from x1 to x0.01. It has a digital display that shows pressure in 0.001 units. The second one is a Granville-Phillips Flow 270 Ion Gauge Controller which senses pressure in the ranges of 10^{-4} torr to 10^{-8} torr. The pressure gauges were placed the first on top of the other and used in tandem, the first one to read the value from the digital display and the second one to check the units. For the first instrument, the input sensor knob was turned to 1K and the resolution knob was turned to x1. The digital pressure value shown in the first instrument was calibrated with the second one such the values could be read together in the scientific notation, with the digital display showing the first two significant digits and the second one showing the exponent part of the value via LED indicators.

For the experiment, **argon gas** was used for producing the plasma arc needed for sputtering. To facilitate as many high energy collisions of gas ions with the target surface as possible, the sputtering gas is chosen of high molecular weight, such as argon (Ar), krypton (Kr), or xenon (Xe). Furthermore, noble gases offer the advantage of being chemically inert. However, for sputtering purposes, argon is widely used as the sputtering gas due to its low cost and medium weight. Argon was available in highly pressurized containers and a nozzle was used for its controlled injection.

Two Kepco APH 500M 0-500 V, 0-40 mA **variable DC voltage power supplies** were used as power supplies for the manganese (Mn) and aluminum (Al) cathodes while a DC variable voltage power supply was used to power the tantalum (Ta) cathode using a Hammond 370LX power transformer.

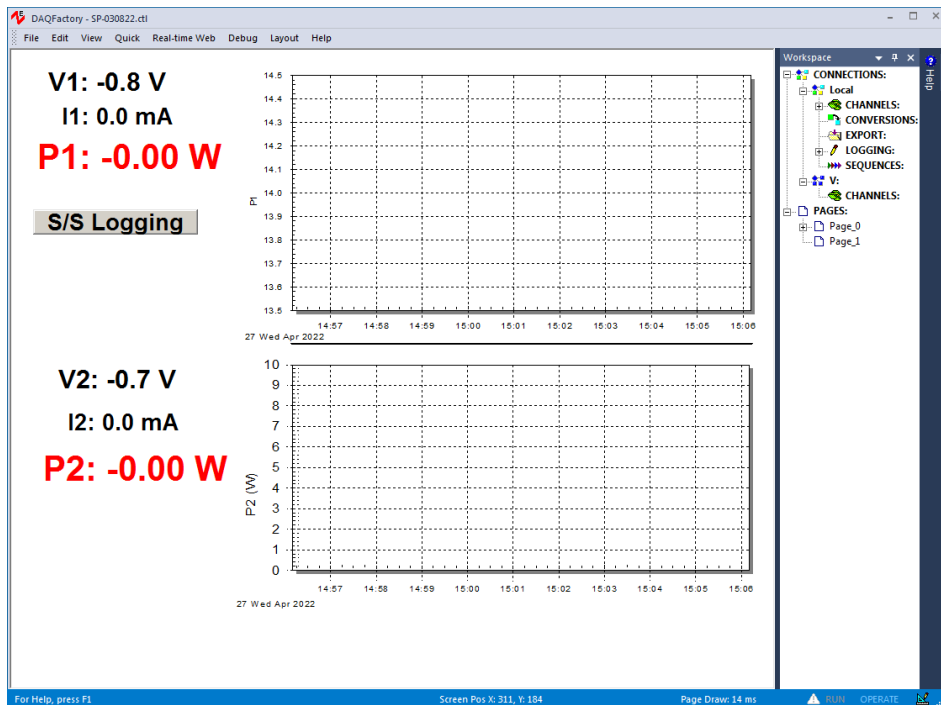


Figure 3: The User Interface in DAQFactory used to read voltage and current values as functions of time for the two cathodes

A LabJack U6 device was used to convert the analog voltages representing the power supply currents and high voltages into digital form, though a USB cable input to the computer. The software used to measure the voltage and current values of the power supplies for the Mn and Al cathodes is **DAQFactory**. The User Interface was as shown in Figure 3. The power P1 was used to denote the power supply to the Al target, whereas the power P2 was used to denote the power supply to the Mn target.

A. II. Annealing

Annealing is a **heat treatment** process by which a material is heated above its **recrystallization** temperature for a set amount of time and then allowed to cool slowly, allowing recrystallization to happen. The heating process allows for atoms to migrate in the crystal lattice and this reduces the number of dislocations, increasing its ductility while decreasing its hardness. In the case of ferromagnetic materials, the magnetic moment saturation, M_s has been found to increase with increase in annealing temperature, T_a till a point after which it decreases with further increase in T_a . In the experiment, the Mn-Al sample before annealing is shown to have a net zero magnetization under external magnetic field, but after annealing it shows ferromagnetic behavior.

A. II. a. Experimental setup

A schematic diagram of the experimental setup for the annealing process is shown in Figure 4. Pictures of the instruments are available in the Appendix.

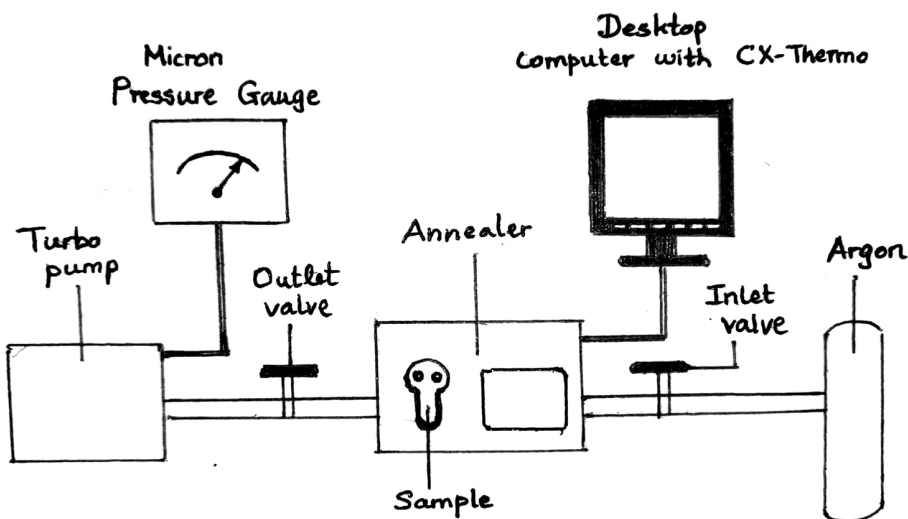


Figure 4: Schematic diagram of the experimental setup for the annealing process

The annealing process takes place in the ULVAC MILA-5000-P-N **Mini Lamp Annealer**, which is a high-temperature type near-infrared lamp annealer. It can reach a maximum temperature of 1200

°C with a maximum heating rate of 50 °C/s. The annealer has a 1/4 inch Swagelok joint inlet connected via a valve to a pressurized cylinder containing **argon gas**.

The annealer also has a 1/4 inch Swagelok joint exhaust outlet connected via a valve to a **turbo pump** used to pump out annealer. The turbo pump used here is the Varian Mini-Task KF40 969-9170 Turbo Pump. It is a compact oil-free bench-top turbo-pumping system. It is used to provide the vacuum inside the annealer. The **software** used to set the annealing temperature, duration, and cool-down is **CX-Thermo**. Its User Interface is shown in Figure 5.

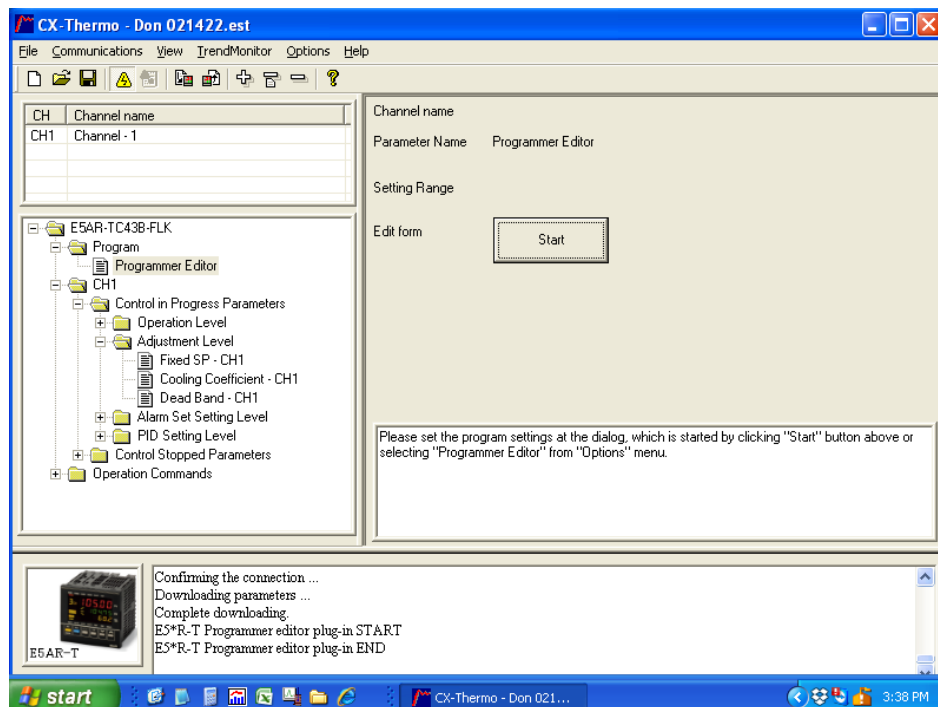


Figure 5: The CX-Thermo User Interface

A. III. Superconducting Quantum Interference Device (SQUID) Magnetometry

The SQUID is a **highly precise** magnetometer used to measure extremely faint magnetic fields. It works on the principle of the **Josephson effect**, where an electric current called a ‘supercurrent’ flows across a device called a ‘**Josephson junction**’ without the need for an electrical potential difference. Josephson junctions arise when two superconductors are placed in proximity with a weak link between them. The weak link can be a thin insulating barrier, a short-section of a non-superconducting metal, or a physical barrier that weakens superconductivity at the point of contact. The SQUID consists of a closed superconducting loop with one or more Josephson junctions in the loop’s current path. Due the quantized state of the superconducting ring and the extraordinary non-linear behavior of the Josephson junction, the SQUID is capable of resolving changes in external magnetic fields that approach 10^{-15} T, yet can be made to operate in fields as large as 7 T [6].

A. III. a. Experimental setup

For the experiment, the commercial **Quantum Design Magnetic Property Measurement System** (MPMS) was used. Figure 6 illustrates the **SQUID magnetometer** design used in the Quantum Design MPMS. It uses a **RF SQUID** with a detection coil composed of four loops, i.e., the upper and bottom coils have a single turn wound clockwise each and the center coil has two turns wound anti-clockwise [6].

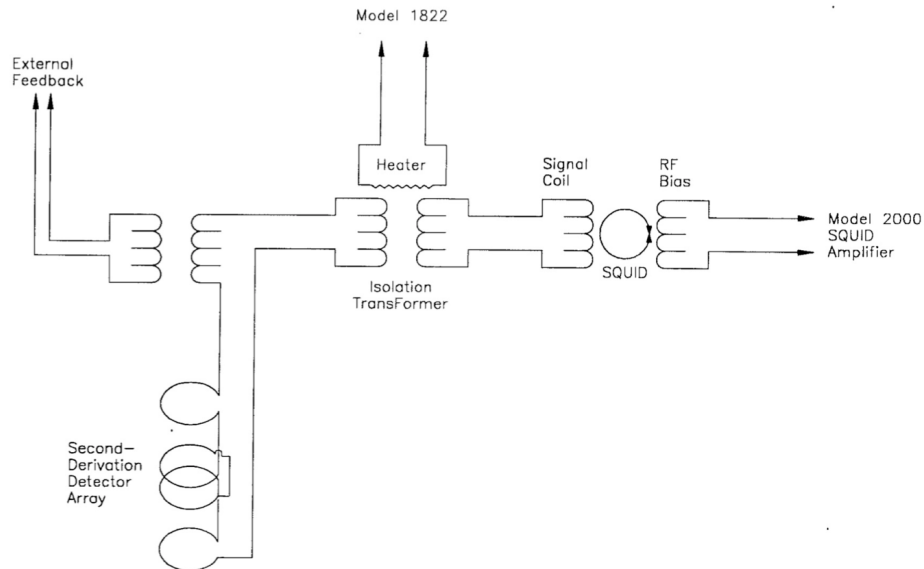


Figure 6: A SQUID magnetometer design used in the commercial Quantum Design Magnetic Property Measurement System [7]

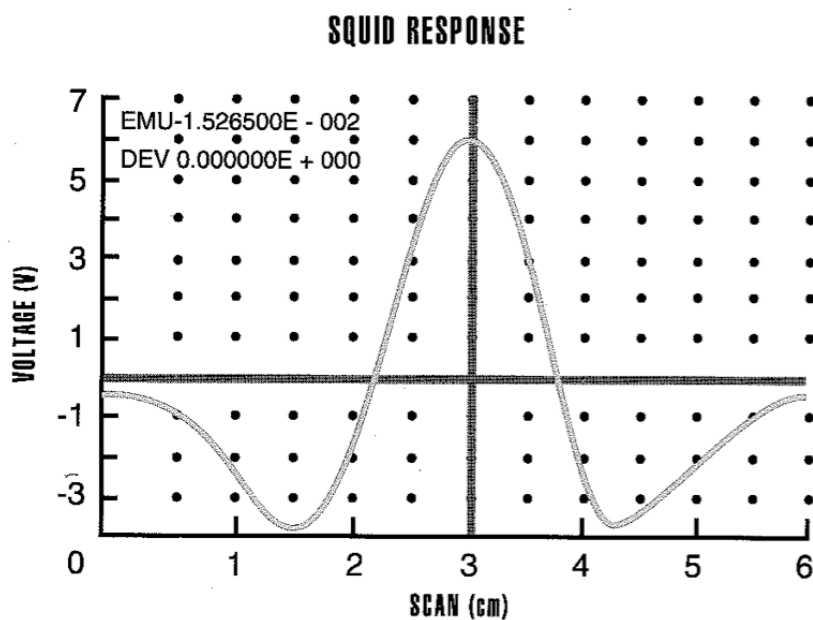


Figure 7: The output voltage of the SQUID as a function of sample position

This design allows for the SQUID to be kept at low magnetic field and temperature while the sample temperature and field are varied [7]. To perform a measurement using the MPMS, the sample is moved back and forth through the superconducting coils. As the sample moves through the coils, its magnetic moment induces a current in the detection coils.

Since the SQUID functions as a **highly linear current-to-voltage converter**, the variations in the current in the detection coils caused by the sample magnetic moment produce an output voltage. The output voltage is measured as a function of position via the RF SQUID, as shown in Figure 7. Pictures of the instruments are available in the Appendix.

A. IV. Scanning Electron Microscopy (SEM)

Scanning Electron Microscopy is an imaging technique that uses a **Scanning Electron Microscope (SEM)** to scan surfaces using a focused beam of electrons. The electrons interact with the surface atoms of the material and produce X-Rays that contain information about the **surface topography** of the sample. For the experiment, the SEM in Lab EG106 of Egan Research Center at Northeastern University was used. The SEM is equipped with an **EDAX X-ray Detector** for measuring the elemental composition via **Energy Dispersive Spectroscopy (EDS)**.

B. Methods

B. I. Physical Vapor Deposition (DC magnetron sputtering)

The process begins by removing the lid and the hollow sputtering chamber cylinder for cathode installation. Three circular disk-shaped cathodes of Mn, Al, and Ta were used for this experiment. After the installation of cathodes, the sputtering chamber cylinder is connected back to the frame. Next, the lid is taken and the silicon (Si) substrate sample is firmly fastened on a piece of titanium metal using the metal clamps on the sputtering stage. A piece of boron carbide (B_4C) is also placed adjacent to the sample and is firmly placed onto the sputtering stage using tape. The lid is then placed on top of the sputtering chamber to close it.

Next, the roughing pump is started to ‘rough out’ the sputtering chamber. To start the roughing process, pump is started and the valve connecting the outlet of the chamber to the roughing pump is opened. The pressure values are read out using the two pressure gauges. The process is continued until the pressure inside the chamber is approximately 100 microns. Once this pressure is reached, the roughing pump is switched off and the valve is closed.

After this, the valve connecting the outlet of the chamber to the cryopump is opened. To get the cryopump to working condition, first it should have been ‘roughed out’ by the roughing pump until a pressure of 2×10^{-7} torr is produced. This takes approximately 26 hours to achieve. The cryopump pressure has an exponential relationship with time (refer to Figure in Appendix).

After the cryopump has been pumped out for 26 hours, the power supplies are adjusted to produce desired value of powers for the cathodes. Since the sputtering rates of the cathodes are proportional to the input power, the concentration of Mn and Al in the thin film can be adjusted by adjusting the

power supplies. Slowly, argon is let in to produce a constant pressure of 5×10^{-7} torr. Argon injection was observed to be correlated with a drop in input powers and constant values of pressure and powers were maintained by careful control of the inlet nozzle. The powers used for growing Manganese and Aluminum were theoretically calculated to be 7.5 W and 14.1 W respectively (refer to Discussion section). The power supplies are set at these values and the values were checked in DAQFactory. The deposition was carried out for 11 minutes and during this time, the injection of argon was controlled by looking at the time varying power values shown in DAQFactory. After the Mn-Al sample was grown, a layer of Ta was grown for 25 seconds on top of the Mn-Al layer as a protective cap at a constant current of 41 mA.

B. II. Annealing

To anneal the sample, clean tweezers are used to carefully place it on a piece of clean titanium metal in the sample holder. The titanium piece protects it from dirt and magnetic dust in the holder. The sample holder has dimensions 20 mm x 20 mm, so the sample is cleaved to a small enough size that it fits in the holder. The sample holder has two screws used to tightly secure the sample inside the annealer. Once the sample is secured, the air is pumped out by the vacuum pump. A micron digital pressure gauge is used to read the pressure in the annealer. Once the pressure gauge reads 0.2 microns, the valve connecting the annealer to the turbo pump is closed. The valve connecting the annealer to the pressurized argon cylinder is slowly opened and argon is let in.

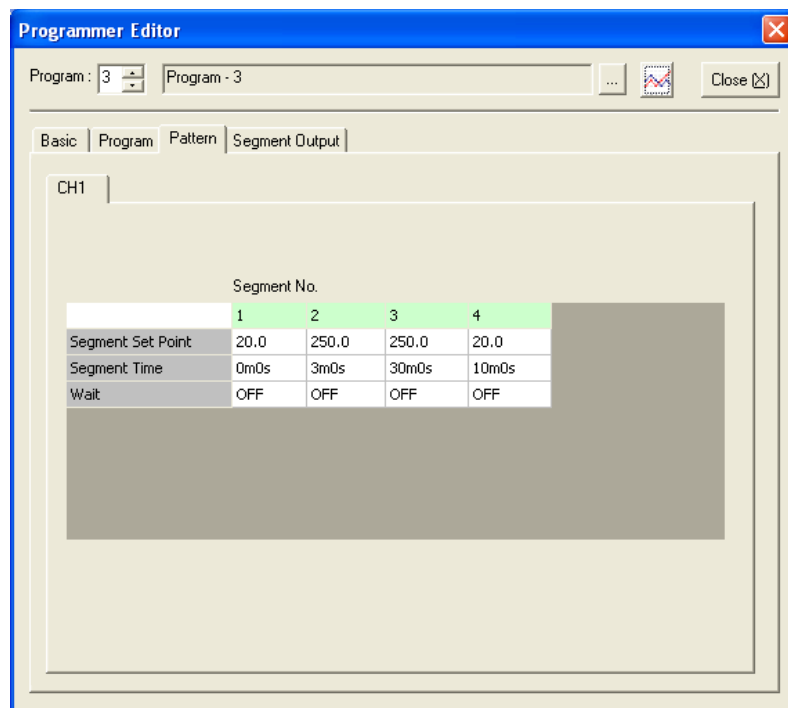


Figure 8: Programmer Editor

Once the annealer is filled with argon, the argon gas valve is closed and the annealer is once again pumped out by the turbo pump. Again, once the pressure reaches 0.2 microns, the turbo pump valve is closed and argon is let in once more, as it was decided that the sample was to be annealed in argon gas. Once this process is done, the machine is switched on. The desktop computer was connected to the annealer using a serial data port called COM7 OMRON K3SC-10 Interface Virtual

COM Port and set to work online. The ‘Programmer Editor’ window is used to set the annealing parameters. It is as shown in Figure 8.

To set the temperature segment parameters, the ‘Pattern’ tab is clicked and the values for ‘Program No.’, ‘Segment Set Point’ and the ‘Segment Time’ are set. Next, under the ‘Basic’ tab, the ‘Program No.’ is set to the same value set in the ‘Pattern’ tab. After this is done, in the Toolbar, the ‘Communications’ button is clicked and the ‘Download Changed Parameters’ option is selected under the ‘Transfer to Device’ option. To transfer the file to the annealer, the ‘Overwrite’ option is selected. This causes the program number on the annealer’s digital display to change to the one set for the file.

Next, the ‘TrendViewer’ tab under ‘TrendMonitor’ option is selected, shown in Figure 9. This opens up a new window and ‘Process Value - CH1’ and ‘Set Point - CH1’ are added to the monitor by clicking the ‘Add Monitor Parameter’ button. Next, under ‘Operation(M)’, ‘Start Monitor’ is clicked to start recording the ‘Process Value’ and ‘Set Point’ in real time. Finally, to execute the file, ‘Execute’ is clicked. This starts increasing the temperature according to the ‘Segment Time’ and ‘Segment Set Point’. Once the annealing process is done, ‘Stop Monitor’ under ‘Operation(M)’ is clicked. After the sample has cooled down to 20 °C, it can be removed from the annealer.

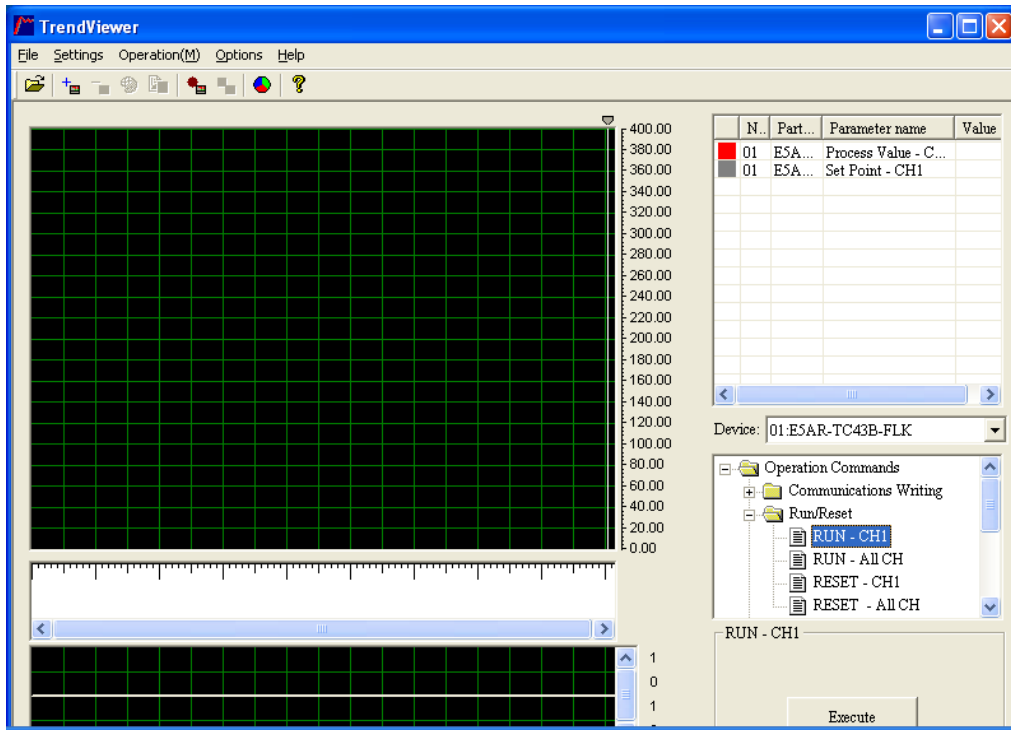


Figure 9: TrendViewer

B. III. SQUID Magnetometry

To perform the scan, the sample is cleaved into small pieces, approximately 5 mm x 5 mm. This is done so that they can fit perfectly into a commercial transparent plastic straw either in the parallel or perpendicular direction. Before the sample can be inserted into the SQUID, it must be vented.

This is done using the software MPMS MultiVu Application. Once the system is purged, the airlock plug can be removed and the long thin rod that functions as the sample holder can be taken out. The sample is then fixed onto the rod using straw adaptors and carefully inserted into the SQUID. Once the airlock plug is placed back, the SQUID automatically asks to enter the sample name. The name is entered and the sample is centered. This centering is crucial as it positions the sample exactly in the middle of the center coils. Once centering is done, the system is ready to execute a sequence. An example of a sequence is shown in Figure 10. The sequence commands are in-built commands which can be copy-pasted from a list of commands.

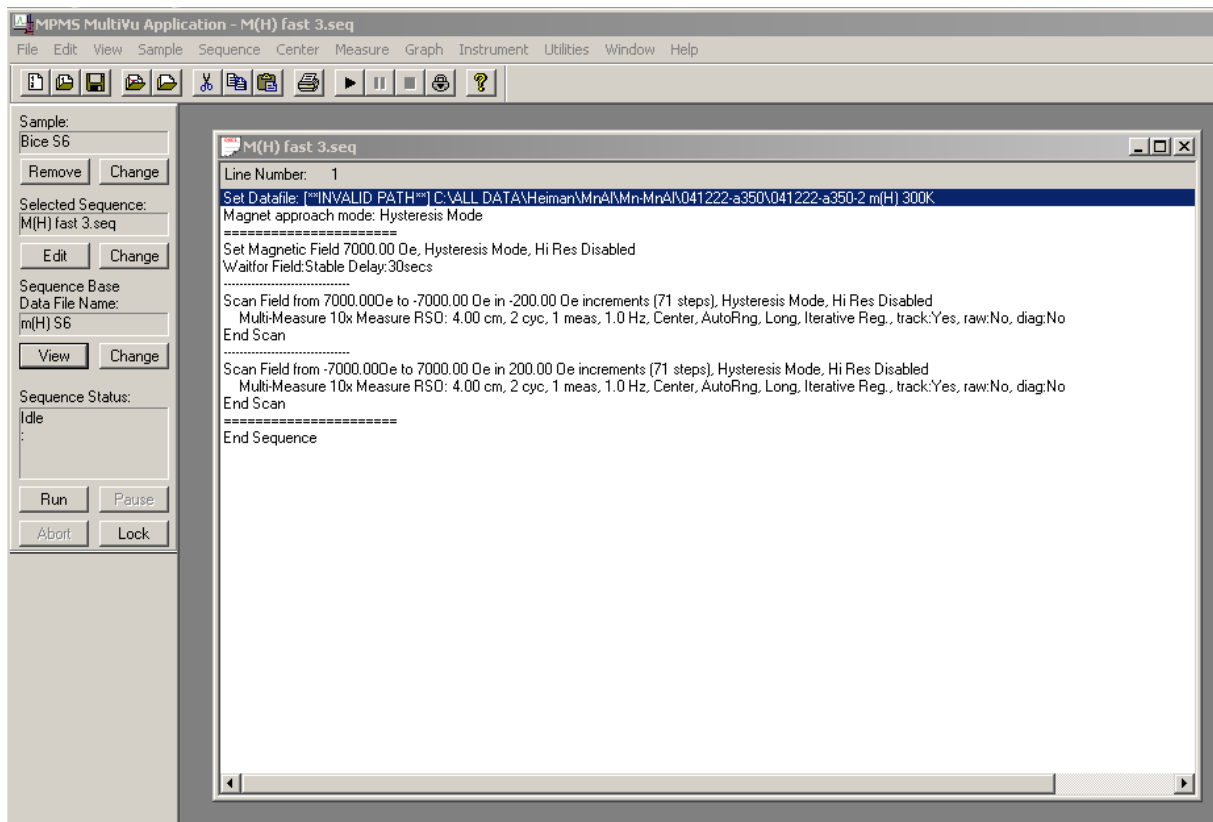


Figure 10: m(H) measurement using the MPMS MultiVu Application

B. IV. Scanning Electron Microscopy (SEM)

To perform the SEM analysis, the boron carbide (B_4C) sample grown alongside the MnAl is used. The B_4C sample is mounted on a stage and made ready. The SEM chamber is vented and the sample is placed inside. The SEM automatically centers the sample and its position is visible to the user via a camera. The software is started and after the file is saved, the process is started. Before the electron beam is allowed to fall on the sample, the camera is switched off as it could deflect the beam. The sample is then moved under the microscope using a ball mouse. Preferred locations are selected and characterization is done by looking at the K peaks. Mn and Al are alone chosen while doing characterization as other elements such as silicon (Si) and oxygen (O) are also shown to be present.

III. Results

A. Physical Vapor Deposition (DC magnetron sputtering)

Three sets of samples were grown. The first sample, named 031122 was grown assuming power values (see Discussion Section) for 60:40 Mn:Al composition.

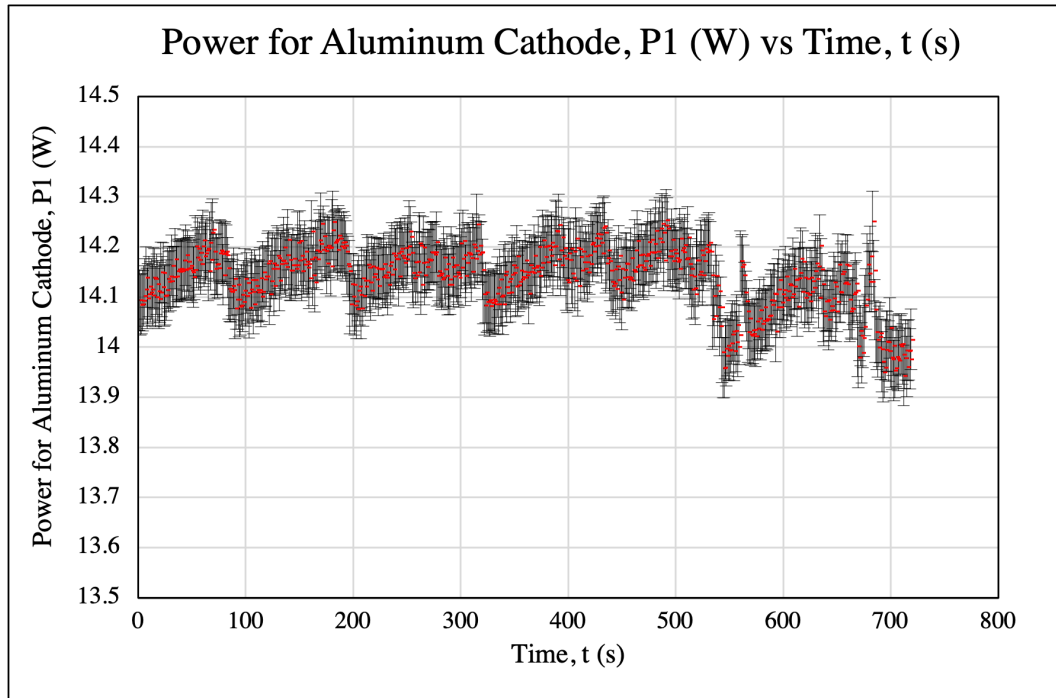


Figure 11: Power for Aluminum Cathode, P1 (W) vs Time, t (s)

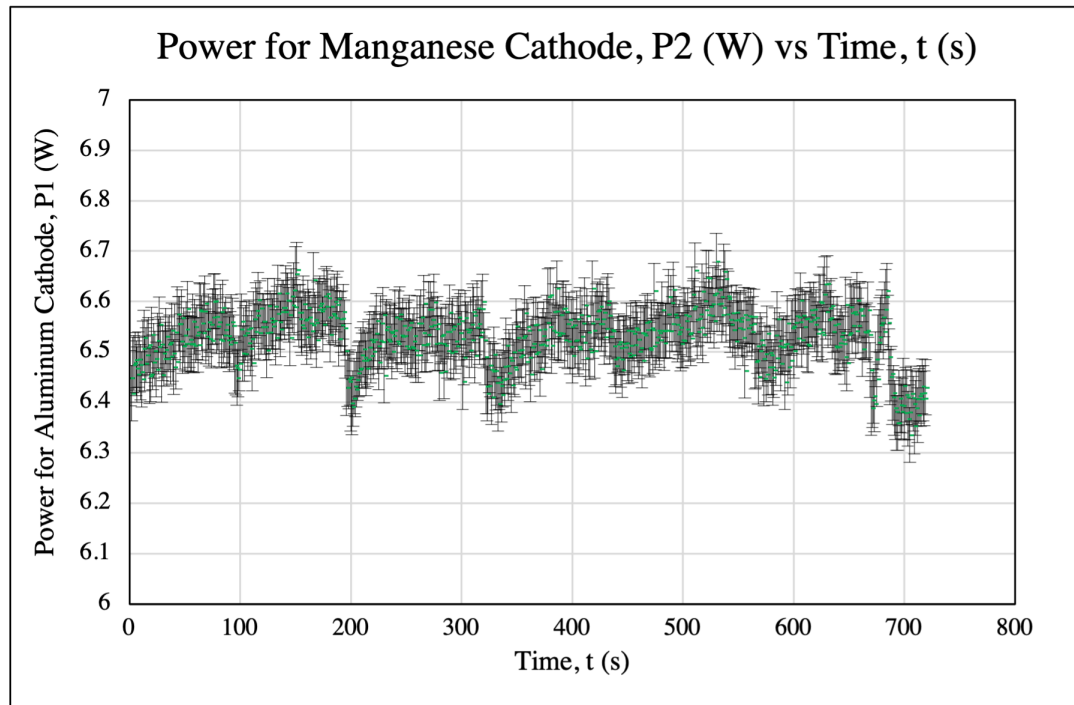


Figure 12: Power for Manganese Cathode, P2 (W) vs Time, t (s)

The second sample, named 031722 was grown assuming the same powers. The third sample, named 041222 was grown assuming new power values for 55:45 Mn:Al composition.

The powers P1 and P2 from the DAQFactory software for sample 041222 are shown in Figure 11 and 12.

B. SQUID Magnetometry

The output of the SQUID Magnetometry is shown in Figures 13 to 17. The error in measurement from SQUID was taken to be 2% of the value of the average magnetic moment [8].

These scans were done at 300 K. The hysteresis loop can be seen in Figure 13 for sample 041222, which is characteristic of a Ferromagnetic material, indicating that the sample has been grown in the tau phase for ferromagnetic behavior. Figure 16 shows the behavior of sample 031122 (MnAl) at 300 K after having been annealed at 200 °C and 250 °C. Figure 17 shows the behavior of sample 031722 (Mn-MnAl) at 10 K. Sample 031722 was a grown as an AFM-FM heterostructure.

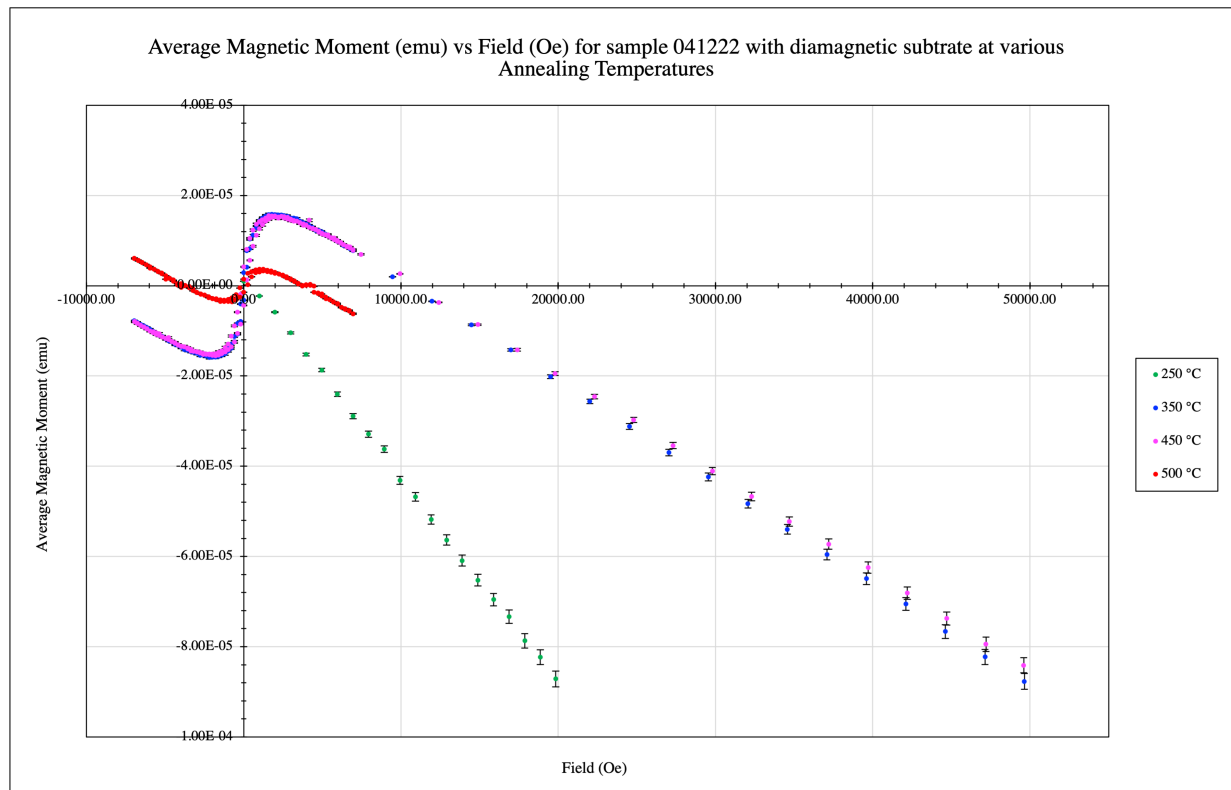


Figure 13: Average Magnetic Moment (emu) vs Field (Oe) at 300 K for sample 041222 with diamagnetic substrate at various Annealing Temperatures

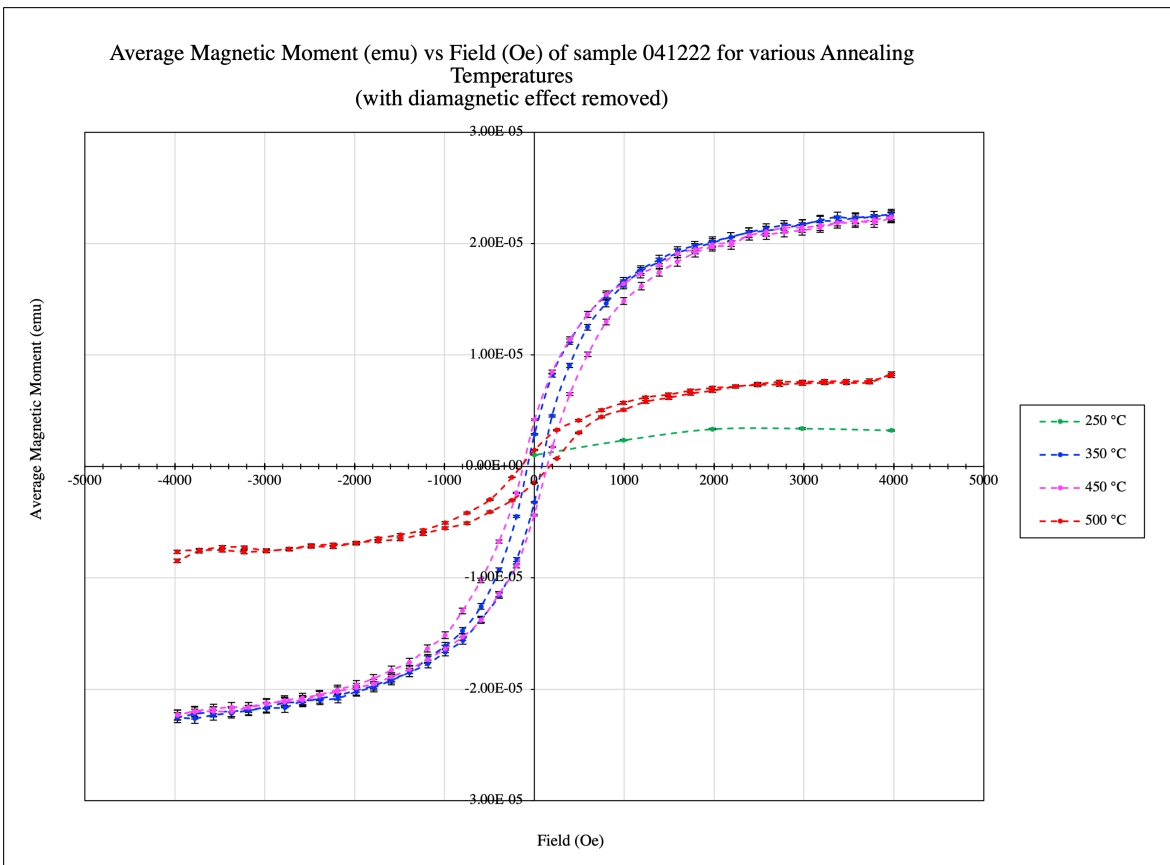


Figure 14: Average Magnetic Moment (emu) vs Field (Oe) at 300 K for sample 041222 for various Annealing Temperatures (with diamagnetic effect removed)

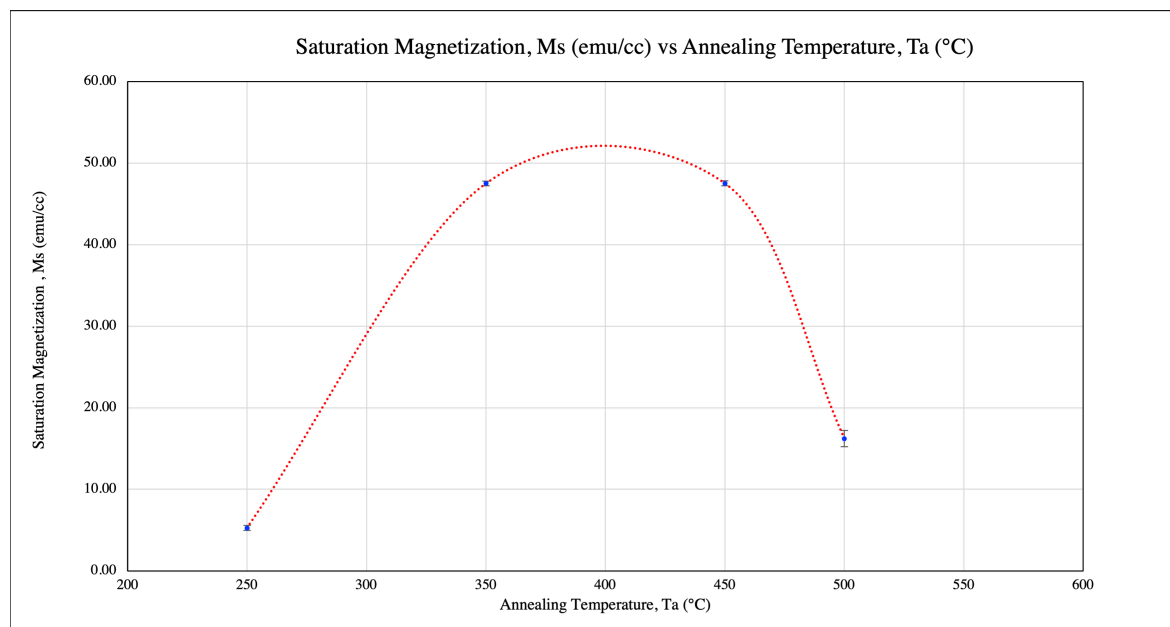


Figure 15: Saturation Magnetization, M_s (emu/cc) vs Annealing Temperature, T_a ($^{\circ}$ C)

Average Magnetic Moment (emu) vs Field (Oe) at 300K for sample 031122 for different Annealing Temperatures

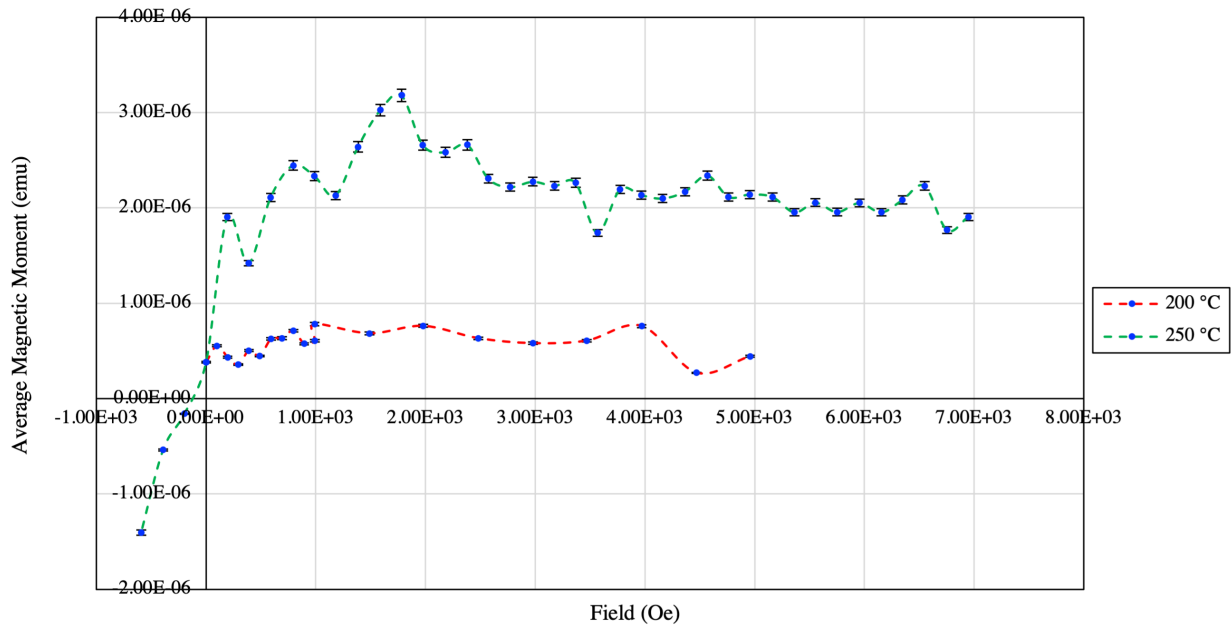


Figure 16: Average Magnetic Moment (emu) vs Field (Oe) at 300K for sample 031122 for different Annealing Temperatures (diamagnetic effect of substrate removed)

Average Magnetic Moment (emu) vs Field (Oe) at 10 K for sample 031722 (Mn-MnAl) annealed at 250 °C

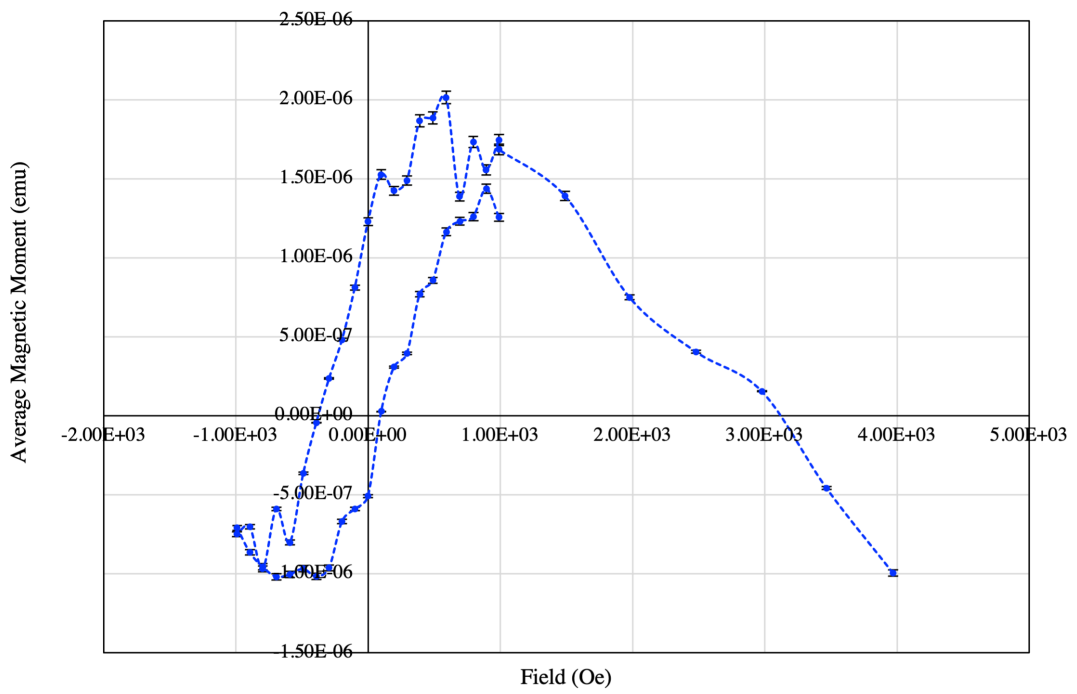


Figure 17: Average Magnetic Moment (emu) vs Field (Oe) at 10 K for sample 031722 (Mn-MnAl) annealed at 250 °C (with diamagnetic effect due to substrate)

C. Scanning Electron Microscopy (SEM)

The results of the SEM analysis are as shown in Figures 18 and 19. Figure 18 showcases the concentration of Mn and Al in sample 031122.

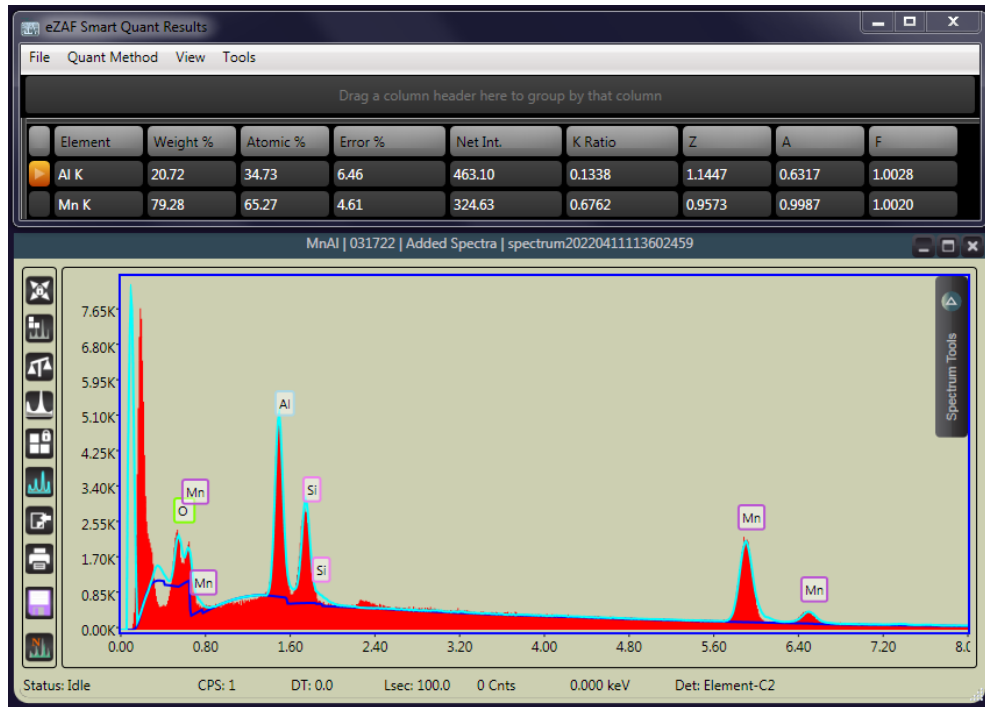


Figure 18: SEM characterization for sample 031122 in the upper region of the sample

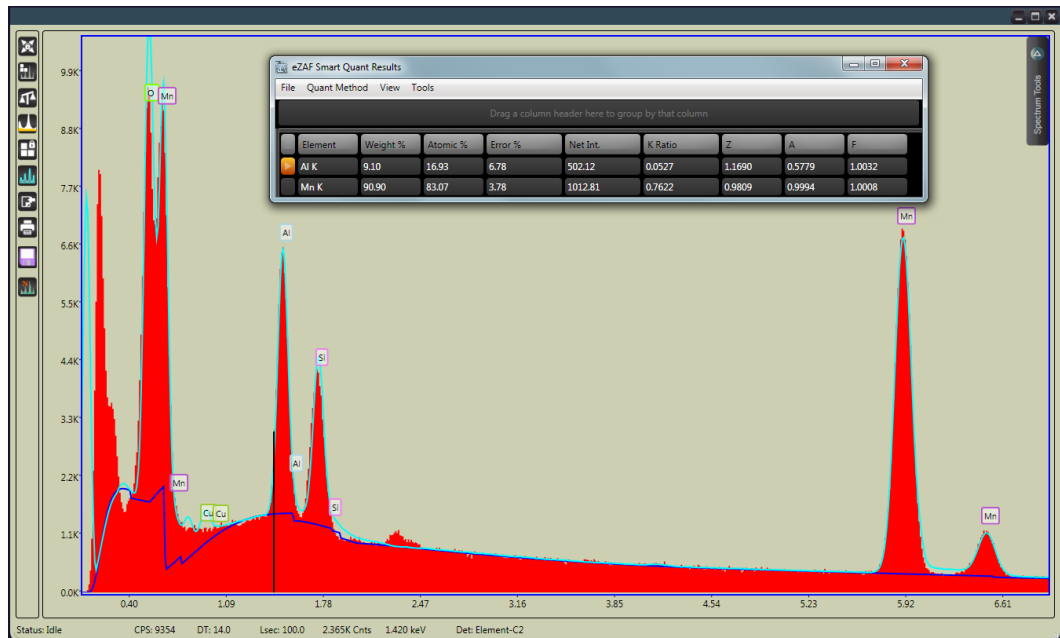


Figure 19: SEM characterization for sample 031722 in the mid region of the sample

Similarly, Figure 19 showcases the concentration of Mn and Al in sample 031722. For both samples, the characterization was done in multiple locations and the average was taken.

IV. Discussion

A. Uncertainty calculations

All uncertainty values were calculated using the **standard deviation** formula:

$$\sigma = \sqrt{\frac{\sum_{i=1}^N (x_i - \bar{x})^2}{N - 1}}$$

B. Power calculation for sample 031122

For the sample 031122, the composition was chosen to be 60:40 Mn:Al. The power values were estimated using a previous synthesized **MnAlGe sample** that was grown for 8 minutes using Mn and AlGe targets with **Mn target power as 6.1 W** and **AlGe target power as 14.1 W**.

Since the deposition of a material is directly proportional to the power supplied and the time for which deposition is carried out, one can produce the following mathematical relationship:

$$x = kP$$

Here, x is the concentration of the target material in the thin film (in percentage), P is power supplied to the target (in Watt), and k is a proportionality constant.

The power for the AlGe target (P_1) was fixed to be 14.1 W, which is the maximum power that the power supplies could provide.

The power for the Mn target (P_2) was calculated as follows:

The Mn:AlGe ratio was assumed to be 50:50 and the proportionality constants k of Al and Ge were assumed to be equal. This assumption allows for replacing Ge in AlGe by Al. Doing so gives us MnAl grown for 8 minutes at a 50:50 Mn:Al ratio.

For a Mn:AlGe ratio of 50:50, the power supplied to the Mn target was 6.1 W. Making the above assumption, we can say that:

$$\frac{x_n}{x_p} = \frac{P_n}{P_p}$$

Here, x_p and P_p are the Mn concentration in MnAlGe and power supplied to the Mn target respectively, and x_n and P_n are the Mn concentration in MnAl sample 031122 and power supplied to the Mn target respectively. The subscripts n and p denote ‘new’ and ‘previous’ samples.

The equation can also be written as $P_n = P_p \cdot \frac{x_n}{x_p}$

Thus, we can calculate P_n as $P_n = \frac{6.1 \times 60}{50} = 7.32$ W.

Thus, the sputtering power supply for Mn was tuned to the constant value of **7.32 W** and sample 031122 was grown for **11 minutes**.

For sample 031122, the experimentally observed average value of P1 and P2 were found to be **14.10 ± 0.07 W** and **7.47 ± 0.06 W** respectively. The experimental value of P2 (Mn) was tuned to be pretty close to the desired theoretical value.

C. SEM analysis for sample 031122

Using SEM to analyze **K peaks in two regions** (upper and lower) on sample 031122, it was found that the actual concentration of Mn:Al was **65.27 : 34.73** in the upper region and **57.17 : 42.83** in the lower region. Figure 18 shows the SEM output for the upper region.

Thus, the experimental value of Mn and Al concentration in sample 031122 were determined to be **(61 ± 6)%** and **(39 ± 6)%**. Due to the fact that only two readings were taken, the uncertainty is pretty large, but nevertheless, this was very close to the theoretical desired value of 60:40 for the Mn:Al ratio.

D. Power calculation for sample 031722

To maintain the 60:40 Mn:Al ratio, sample 031722 was also grown with the same power for the Mn target.

The sample 031722 was grown assuming the same powers as it also used the 60:40 Mn:Al ratio. After the growth of MnAl for 11 minutes, an **additional layer of Mn** was deposited for **20 minutes** using the same power supply.

For sample 031722, the experimentally observed average value of P1 and P2 were found to be **14.1 ± 0.1 W** and **7.49 ± 0.05 W** respectively. The experimental value of P2 (Mn) was tuned to be pretty close to the desired theoretical value.

E. SEM analysis for sample 031722

Using SEM, **K peaks in three regions** (upper, mid, and lower) were analyzed on sample 031722. It was found that the actual concentration of Mn:Al was **82.6 : 17.4** in the upper region and **83.07 : 16.93** in the mid region, and **83.66 : 16.34** in the lower region. Figure 19 shows the SEM output for the mid region.

Thus, the experimental value of Mn and Al concentration in sample 031722 were determined to be **(83.1 ± 0.5)%** and **(16.9 ± 0.5)%** respectively. Since three readings were taken, the uncertainty is much smaller than the one obtained for sample 031122.

F. Power calculation for sample 041222

F. I. Calculating Mn concentration in the FM MnAl layer in sample 031722

The sample 041222 was decided to be grown in the **55:45 Mn:Al ratio** and thus the value for the new power supplied to the Al target was calculated using the same method as above.

Since the actual concentration obtained from SEM analysis on sample 031722 was much more accurate than the one obtained from sample 031122, the former is taken to calculate the new power for sample 041222.

Since sample 031722 had $(83.1 \pm 0.5)\%$ Mn grown for 31 minutes, the amount of Mn grown for 11 minutes is calculated by:

$$\text{Amount of Mn grown for 11 minutes} = \frac{(83.1 \pm 0.5)(11)}{31} = (29.5 \pm 0.2)\%$$

Since sample 031722 had $(16.9 \pm 0.5)\%$ Al grown for 11 minutes, the actual ratio of the FM MnAl layer can be found as follows:

$$\text{Actual amount of Mn in the FM MnAl layer} = \frac{(29.5 \pm 0.2)}{(29.5 \pm 0.2) + (16.9 \pm 0.5)} = \frac{(29.5 \pm 0.2)}{(46.4 \pm 0.7)}$$

Using **Propagation of Errors formula**, we can calculate the uncertainty as follows:

$$\sigma_x = \sqrt{(\sigma_u)^2 \left(\frac{\partial x}{\partial u} \right)^2_{(\bar{u}, \bar{v})} + (\sigma_v)^2 \left(\frac{\partial x}{\partial v} \right)^2_{(\bar{u}, \bar{v})}}$$

Here, $\bar{x} = \frac{\bar{u}}{\bar{v}} = \frac{29.5}{46.4} \approx 0.636$, $\sigma_u = 0.2$, $\sigma_v = 0.7$.

Since $x = \frac{u}{v}$, $\frac{\partial x}{\partial u} = \frac{1}{v}$, and $\frac{\partial x}{\partial v} = -\frac{u}{v^2}$,

$$\text{This implies that } \sigma_x = \sqrt{(0.04) \left(\frac{1}{46.4} \right)^2 + (0.49) \left(\frac{29.5}{(46.4)^2} \right)^2} = \frac{\sqrt{0.04 + (0.49)(0.40)}}{46.4}$$

$$\text{or } \sigma_x = \frac{0.49}{46.4} \approx 0.01.$$

Thus, we found the actual amount of Mn in the FM MnAl layer to be **(63.6 ± 1.0)%**. Then, the actual amount of Al in the FM MnAl layer would be **(36.4 ± 1.0)%**.

F. II. Calculating new power value for Mn target for sample 041222

For 031722, the experimentally observed average values of P1 (Al) and P2 (Mn) were found to be 14.1 ± 0.1 W and 7.49 ± 0.05 W.

Using these values, the new power for sample 041222 was calculated as follows:

$$P'_n = \frac{(7.49 \pm 0.05) \times 55}{(63.6 \pm 1)} = \frac{(411.95 \pm 2.75)}{(63.6 \pm 1)}$$

Again using **Propagation of Errors formula**, we can calculate the uncertainty as follows:

Here, $\bar{x} = \frac{\bar{u}}{\bar{v}} = \frac{411.95}{63.6} \approx 6.477$, $\sigma_u = 2.75$, $\sigma_v = 1$.

Since $x = \frac{u}{v}$, $\frac{\partial x}{\partial u} = \frac{1}{v}$, and $\frac{\partial x}{\partial v} = -\frac{u}{v^2}$,

This implies that $\sigma_x = \sqrt{(2.75)^2 \left(\frac{1}{63.6}\right)^2 + \left(\frac{411.95}{(63.6)^2}\right)^2} = \frac{\sqrt{49.516}}{63.6} \approx 0.11$

Thus, we found the new power value for the Mn target for sample 041222 to be **6.48 ± 0.11 W**.

As seen in Figure 12, the average value of P2 (Mn) for sample 041222 was found to be **6.53 ± 0.05 W** which is pretty close to the derived value. Furthermore, as seen in Figure 11, the average value of P1 (Al) for sample 041222 was found to be **14.14 ± 0.06 W**.

G. SQUID Magnetometry for sample 031122

Figure 16 shows the effect of annealing on the magnetization (average magnetic moment) of the sample. The sample was synthesized in the ratio of Mn:Al of **(61 ± 6) : (39 ± 6)** which **does not produce a τ phase** (ferromagnetic phase). Hence the magnetic moments are very small. It can also be noted that there is randomness in the curve and it is not completely flat. This is because the sample is not ferromagnetic and has magnetic dipole spins oriented in random directions.

H. SQUID Magnetometry for sample 031722

Figure 17 shows the B-H curve of sample 031722 which is an AFM-FM heterostructure (Mn-MnAl). It can be noted that the **exchange anisotropy is not seen** in this sample. This is because the FM layer of the sample was grown in a ratio similar to that of sample 031122, i.e., **(63.6 ± 1.0) : (36.4 ± 1.0)**. This ratio does not produce τ phase for the MnAl system and therefore, the heterostructure does not exhibit exchange bias.

I. SQUID Magnetometry for sample 041222

Figure 13 and 14 show the B-H curve of sample 041222. It can be seen that the B-H curve of this sample exhibits hysteresis and therefore is ferromagnetic. This is because this sample was grown in

a proportion noted to produce τ phase in Mn-Al systems, i.e., **55:45 for the Mn:Al ratio**. Figure 13 shows negative slope in the curve produced by the weakly diamagnetic Si substrate. This effect can be removed by taking a regular linear region of points and analyzing the negative slope. The negative slope can be made positive by inverting the sign and a new linear function of the Field can be produced. This linear function upon addition to the existing data points removes the negative slope.

Figure 13, 14, and specifically 15 show the effect of annealing on the FM thin film sample. The Saturation Magnetization (M_s) as a function of Annealing Temperature (T_a) seems to follow a kind of inverted parabolic curve. M_s first increases with increase in T_a until it peaks at around $400\text{ }^{\circ}\text{C}$ (given by the fit in Figure 15), beyond which it decreases with further increase in T_a . This indicates that there is a '**Best Annealing Temperature**' for the sample, here, projected to be **around $400\text{ }^{\circ}\text{C}$** .

J. Scanning Electron Microscopy (SEM)

For this process, the **boron carbide (B₄C)** sample grown alongside the MnAl is used. This is because the latter's Si substrate produces such a large peak due to much larger thickness than the thin film that it becomes very difficult to find the concentration of the thin film elements. During characterization, other elements such as Si and O are present either due to dust or accidental errors in the software.

V. Conclusion

Thus, three different MnAl thin film samples were grown on a silicon substrate using DC magnetron sputtering and the effect of annealing on their magnetic properties was investigated using SQUID magnetometry. Moreover, SEM was used to examine the concentration of Mn and Al in the three samples.

VI. Appendix

The actual photos of experimental setups and instruments are available in this section.

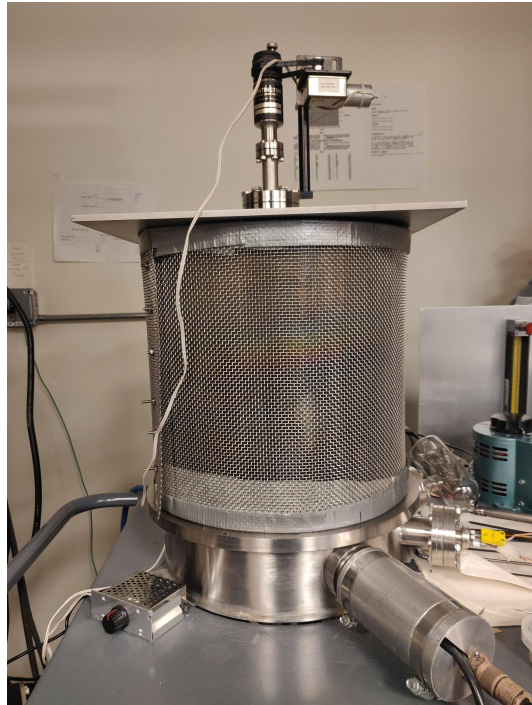


Figure 20: The Sputtering Chamber

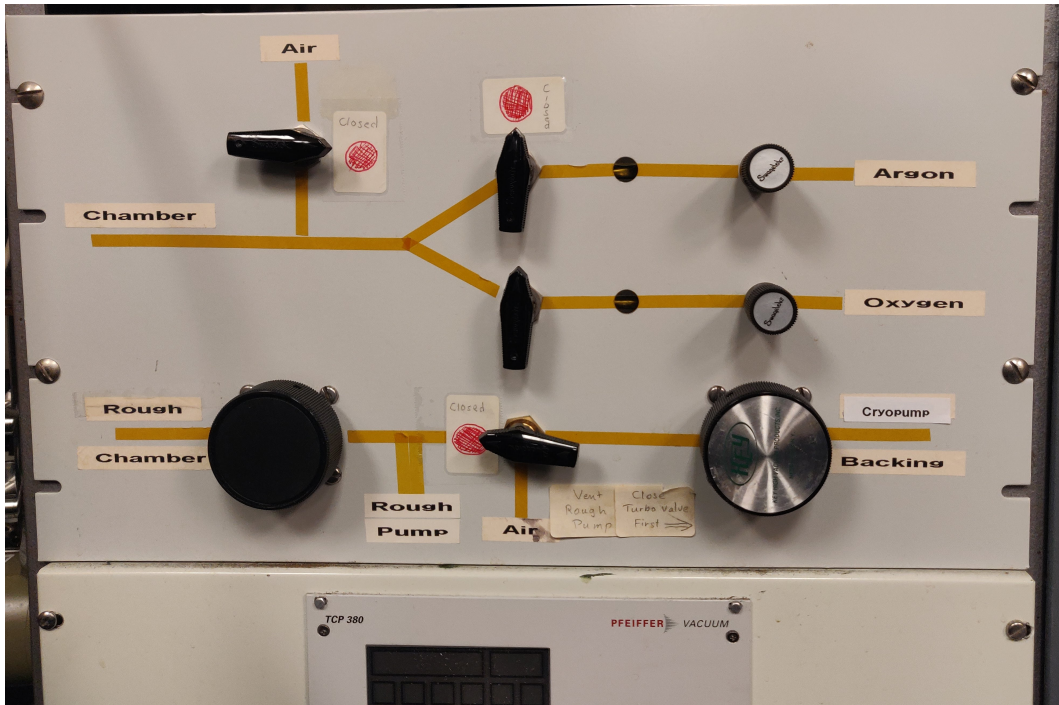


Figure 21: The Valves and Nozzles for the Sputtering Process

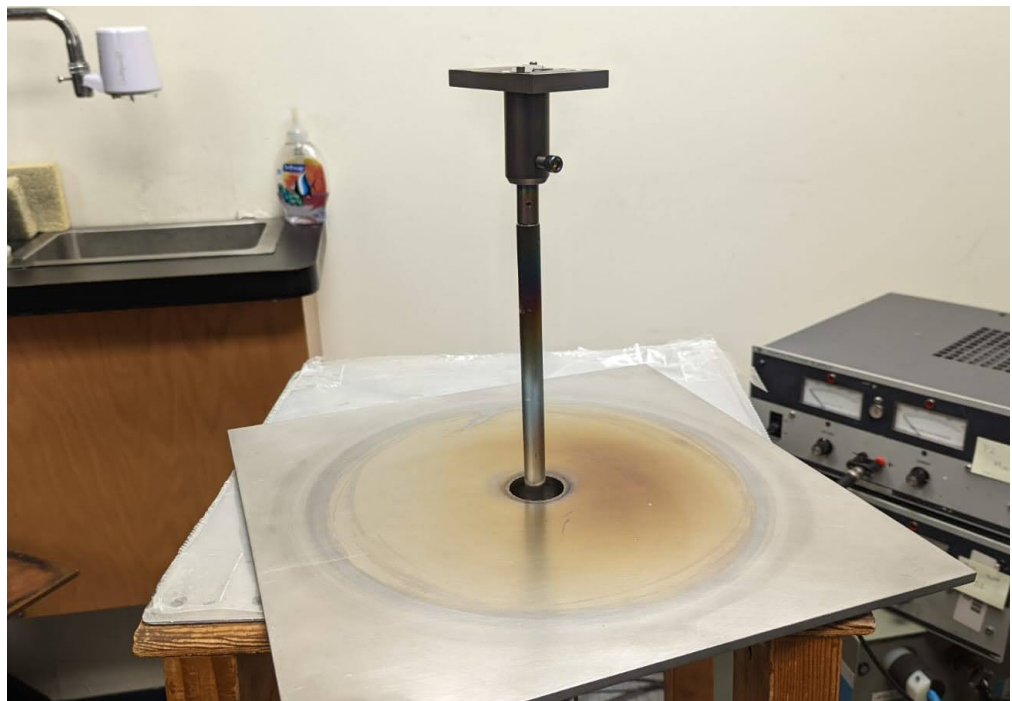


Figure 22: The Sputtering Stage on the Lid

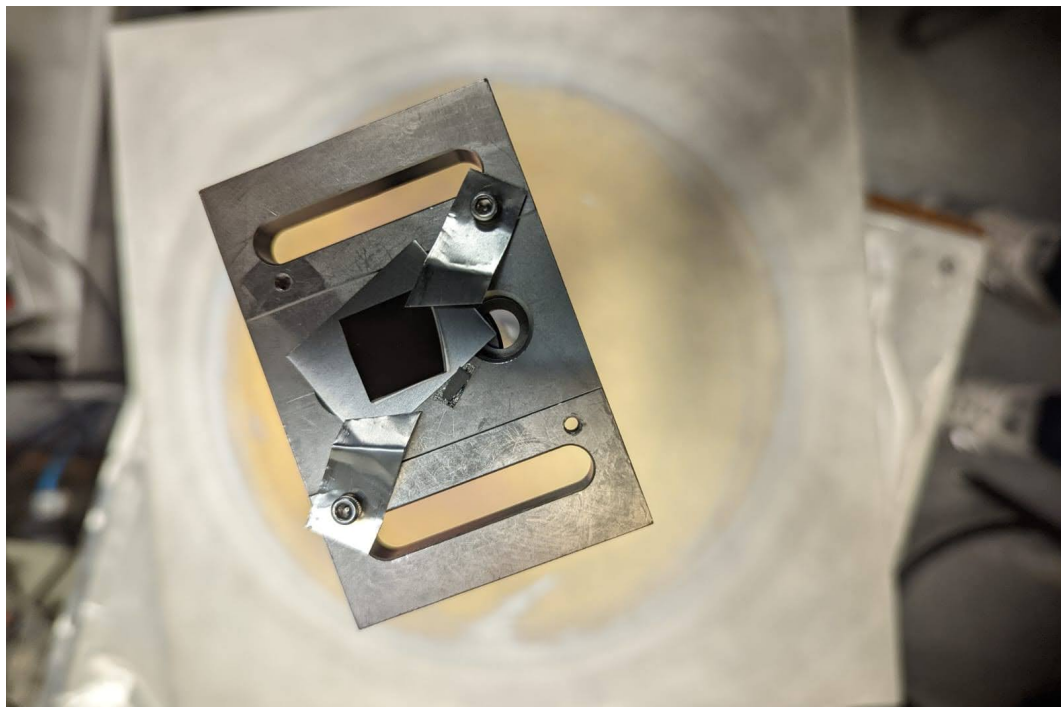


Figure 23: A close-up look of the Si substrate and B₄C piece on a clean Ti plate

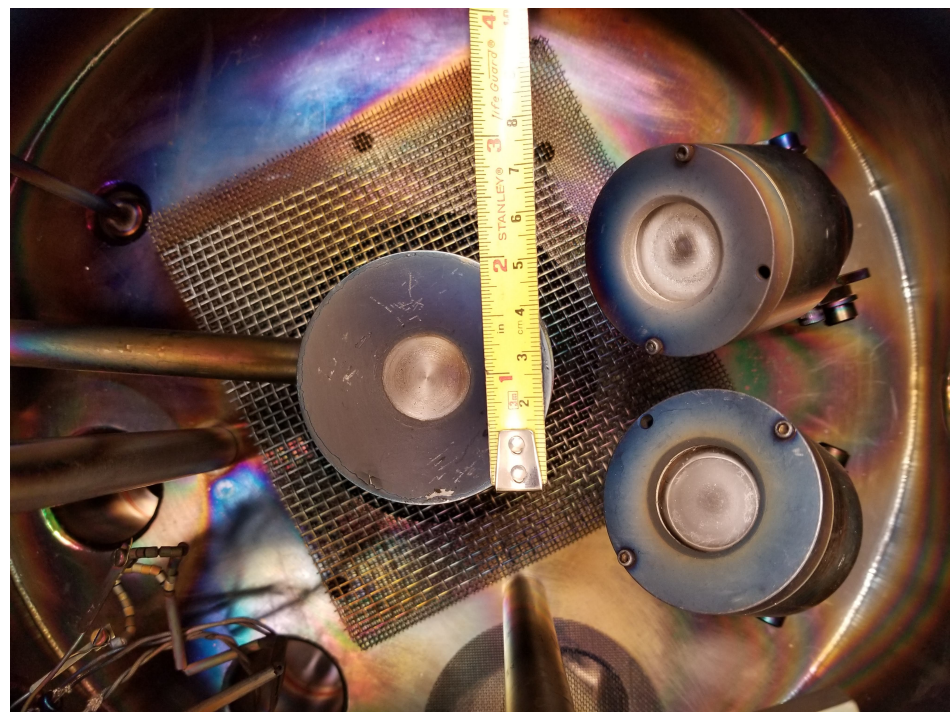


Figure 24: The three Targets inside the Sputtering Chamber

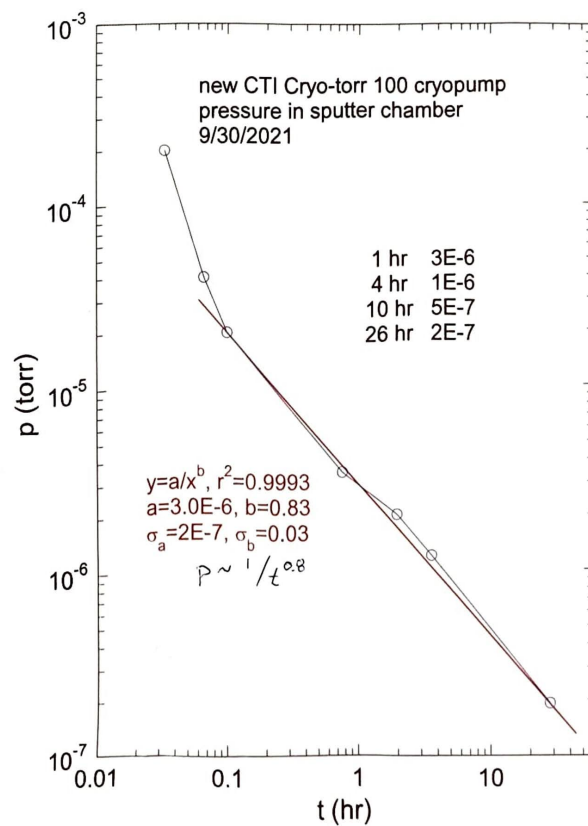


Figure 25: Cryopump Pressure (torr) vs Time (hour)



Figure 26: The two Pressure Gauges



Figure 27: Power Supplies for Mn and Al

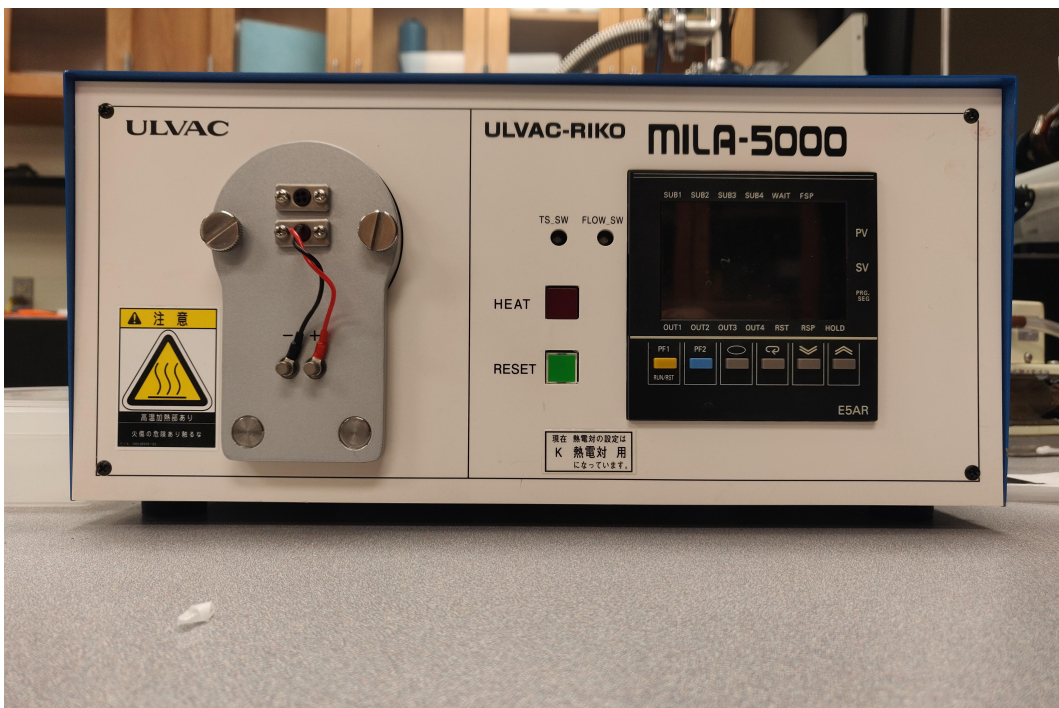


Figure 28: The Mini Lamp Annealer



Figure 29: Turbo pump used to produce vacuum in the Annealer



Figure 30: Sample Holder in the Annealer

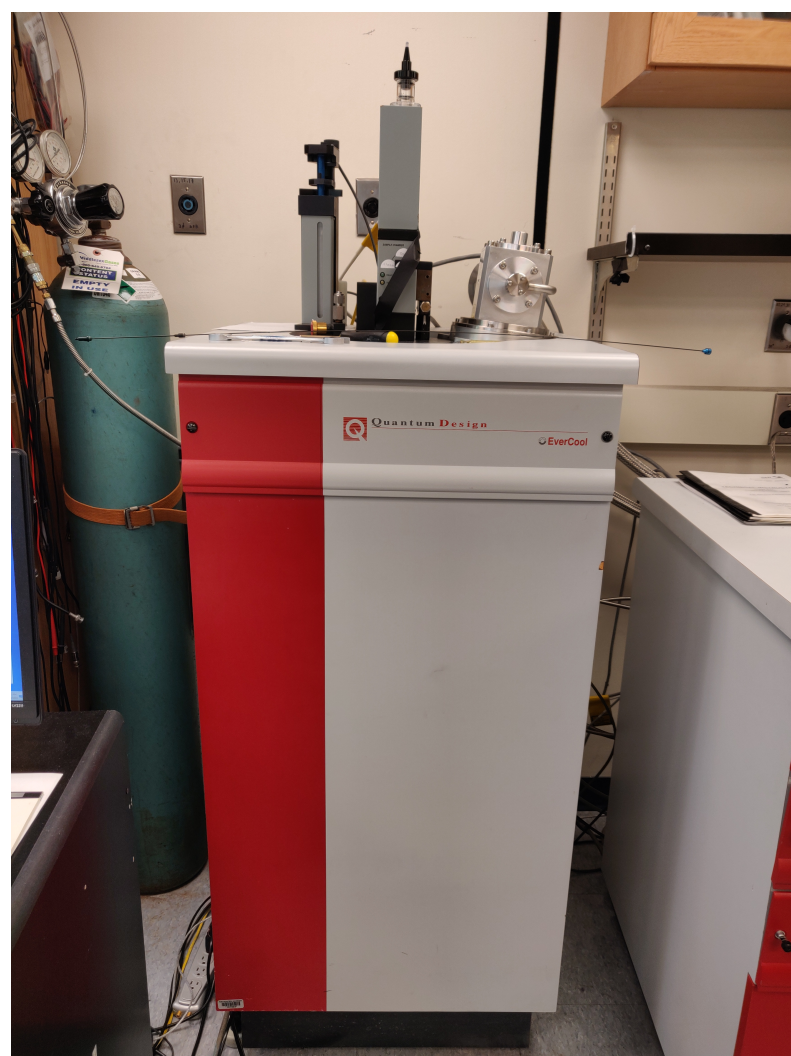


Figure 31: Quantum Design's MPMS with RF SQUID

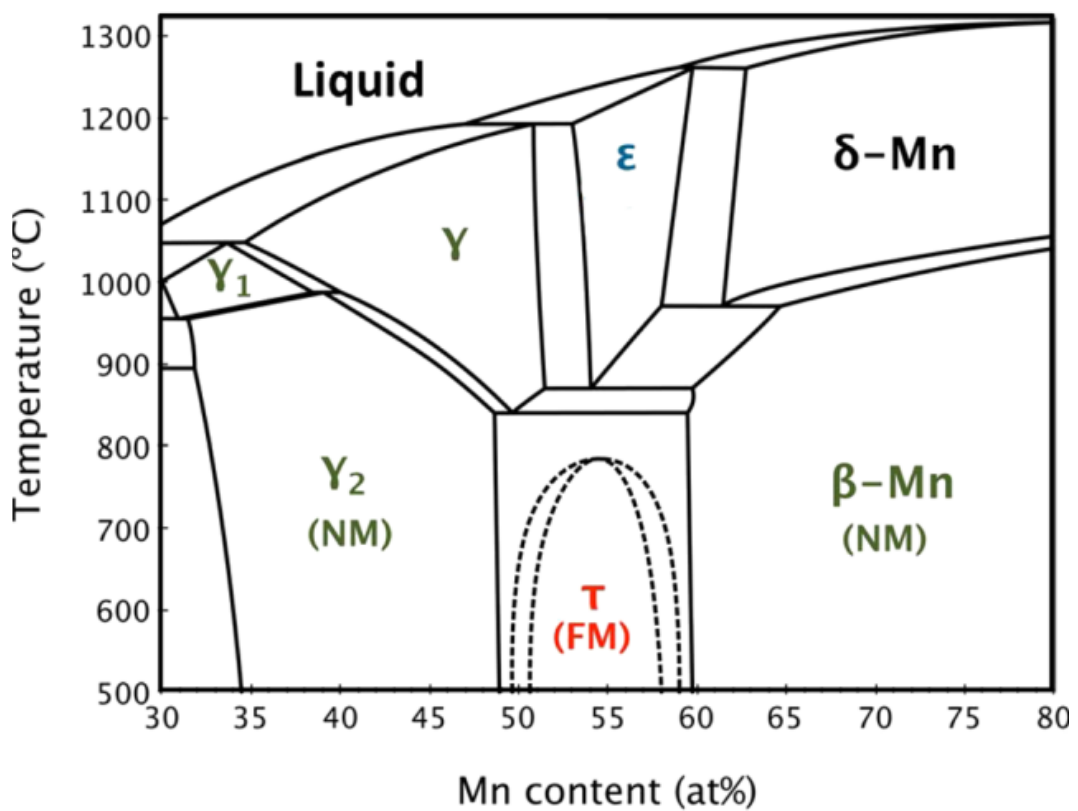


Figure 32: Phase diagram of the Mn-Al system [9]

VII. References

1. Kono, Hiroshi. "On the Ferromagnetic Phase in Manganese-Aluminum System." Journal of the Physical Society of Japan 13 (1958): 1444-1451.
2. Duan, Caiyun et al. "The structural and magnetic properties of τ -MnAl films prepared by Mn/Al multilayers deposition plus annealing." Materials Science and Engineering B-advanced Functional Solid-state Materials 162 (2009): 185-188.
3. Blachowicz, T.; Ehrmann, A., Exchange Bias in Thin Films—An Update, *Coatings* **2021**, *11*, 122.
4. <https://angstromengineering.com/tech/magnetron-sputtering/>
5. http://www.msi-pse.com/magnetron_sputtering.htm
6. McElfresh, M., Fundamentals of Magnetism and Magnetic Measurements Featuring Quantum Design's Magnetic Property Measurement System, **1994**, San Diego, CA, Quantum Design Inc., Purdue University
7. Kraft, Aaron, Christoph Rupprecht, and Yau-Chuen Yam. "Superconducting Quantum Interference Device (SQUID)." *UBC Physics* (2017)
8. Zhou, Chunxia, Tongkui Li, Xianshun Wei, and Biao Yan. 2020. "Effect of the Sputtering Power on the Structure, Morphology and Magnetic Properties of Fe Films" *Metals* 10, no. 7: 896.
9. Zhu, Lijun & Nie, Shuaihua & Zhao, Jianhua. (2013). Recent progress in perpendicularly magnetized Mn-based binary alloy films. *Chinese Physics B*. 22. 118505. 10.1088/1674-1056/22/11/118505.

